# A Hierarchical Circuit-Level Design Methodology for Microelectromechanical Systems

*Gary K. Fedder and Qi Jing*[1]

**Abstract**

*A circuit-level methodology for hierarchical design and nodal simulation of microelectromechanical systems (MEMS) is presented. A layout-based schematic view is introduced as a geometrically intuitive MEMS representation that is transformed into a schematic suitable for behavioral simulation. As examples of the design methodology, suspended-MEMS inertial sensors, resonant actuators and filters are designed using a small set of geometrically parameterized plate, beam, gap and anchor elements. Effects of manufacturing variations are evaluated by simply changing parameter values of the elements.*

## 1: Introduction

Microelectromechanical systems (MEMS) are sensor and actuator systems made from microelectronic batch fabrication processes. Futuristic applications of MEMS, such as inertial navigation systems, high-density data storage, DNA analysis systems, and wireless distributed sensor networks, provide tantalizing opportunities for commercialization. However, successful design and manufacture of these kinds of mixed-technology systems is currently very difficult. Single-chip and hybrid versions of these systems will require integration of digital and analog electronics with tens to thousands of mechanical structures, electromechanical actuators, and various sensing elements (*e.g.,* capacitive transducers for motion sensing). One requirement for successful large-scale system design is the formation of stable MEMS processes with access to reliable materials characterization. A second requirement is for computer-aided design (CAD) tools to support rapid top-down design of systems involving physical interactions between mechanical, electrostatic, magnetic, thermal, fluidic, and optical domains.

---

1. Manuscript received __________. The authors are affiliated with the Department of Electrical and Computer Engineering at Carnegie Mellon University, Pittsburgh, PA 15213-3890. G. K Fedder is also affiliated with The Robotics Institute, Carnegie Mellon University, Pittsburgh, PA. The research effort is sponsored by the Defense Advanced Research Projects Agency under the Air Force Research Laboratory, Air Force Materiel Command, USAF, under grant number F30602-96-2-0304 and in part by a National Science Foundation CAREER Award MIP-9625471.

MEMS design needs are similar to those driving advances in analog and microwave system CAD. As is the case with pure analog design, the existence of hierarchical cell design methodologies, mixed-technology simulators, layout synthesis tools, and design-rule checking will enable MEMS engineers to build larger systems and allow them to concentrate on higher-level design issues.

Currently, most MEMS system-level design is accomplished by modeling entire microelectromechanical components as single behavioral entities having no lower hierarchical level in design. Specific macromodels are usually generated through direct numerical simulation (*e.g.,* finite element analysis or boundary-element analysis) with fitting of results to appropriate analytic functions. An alternative technique employs pattern matching with arbitrary inputs to generate abstract macromodels [1]. Numerical simulation tools that are tailored for MEMS bottom-up modeling are available from several companies [2][3][4]. Generalized techniques have recently been developed for rapid modeling of micromechanical components with electrostatic actuation [5]. Physical effects can be modeled with high accuracy, however for any change in geometric parameters or topology, new models must be created, which slows design iteration. There is no established method for general reuse of the macromodels, or for generating layout from the behavioral representation.

Realization of complex MEMS with more than 1,000 micromechanical elements will require a hierarchical approach to design, a concept borrowed directly from VLSI and analog circuit areas. Reusable behavioral models with geometric parameters may be pre-defined for a finite set of elements. In particular, micromechanical structures can be broken down into hierarchical building-block components. At the lowest level of this hierarchy are plate masses, beam springs, electrostatic air-gaps and anchors. This hierarchical level is analogous to circuit design using transistors, resistors, capacitors and inductors.

In contrast to electrical simulation, MEMS simulation requires inclusion of geometric and layout position parameters since the micromechanical behavior is directly linked to shape of components, and, in the case of inertial sensors, is linked to absolute layout position. The advantages of a hierarchical circuit-level methodology for MEMS are the reusability of the parametric models, the interoperability with electronic circuit representations and the ability to generate layout from the electromechanical components. Macromodels at the lowest level in the hierarchy can be formed *ad hoc* without loss of generality in simulations, because of the finite number of reusable components which form the basis of a very large and useful design space. Modeling intervention during design iterations is only required when a designer insists on device topologies that cannot be constructed from parts in the library.

The hierarchical circuit-level representation for MEMS developed at Carnegie Mellon is called NODAS, for Nodal Design of Actuators and Sensors [6]. Behavioral models of MEMS elements are currently implemented in Analogy MAST® with simulation in Saber® [7][1]. Similar hierarchical macromodels and nodal simulations have been developed in SPICE-like representation with simulation in MATLAB (called SUGAR) by Pister [8][9], in MAST with simulation in Saber by Lorenz [10][11], and partly commercialized [12]. The main distinctions between these efforts are in the nodal representation of position and displacement, in the detailed models, and in the solvers used.

The circuit-level representation is applicable to all MEMS technologies. We begin with an overview of suspended surface-micromachined structures, the technology currently supported by NODAS. A discussion of the underlying models for the basic components is presented, followed by example simulations of a microresonator, a micromechanical bandpass filter, and a lateral capacitive accelerometer.

## 2: Surface Micromechanics

A relatively mature manufacturing technology in MEMS is surface micromachining, as exemplified by the recent success of commercial accelerometers for automotive airbag deployment [13][14] and digital mirror displays for high-fidelity video projection [15]. Successful design and manufacturing of these devices required years of effort, partly due to a lack of adequate system-level MEMS design tools.

The availability of accumulated design expertise, stable fabrication services, and electromechanical CAD modeling tools has made the suspended-MEMS technology a suitable candidate for development of circuit-level design tools for MEMS. Our discussion of hierarchical design is restricted to suspended MEMS, however the concepts apply to other technologies, such as high-aspect-ratio silicon structures.

The polysilicon (thin-film polycrystalline silicon) surface-micromachining process was originally developed in parallel by researchers at U. C. Berkeley, MIT, and Bell Labs, and is commercially available in the Multi-User MEMS Process service (MUMPs) from MCNC [16]. In this process, the micromechanical components are made entirely from a homogeneous, conducting, 2 μm-thick polysilicon film. The movable microstructure is fixed to the substrate through anchor points, which

---

1. MAST is a registered trademark of Analogy, Inc. Saber is a registered trademark of American Airlines, Inc., licensed to Analogy, Inc.

also act as electrical vias. The 2 μm air-gap separation, $g$, between the structures and the substrate is formed by wet etching a sacrificial oxide film under the structure.

The microresonator shown in Fig. 1 is a popular polysilicon MEMS device, first described and analyzed by Tang [17]. It is used in high-quality-factor resonator oscillators and bandpass filters [18], as a resonant actuator for stepper motor drives [19], and as a mechanical characterization test structure to measure Young's modulus of thin films.

The central shuttle mass suspended by two folded-beam flexures forms a mechanical mass-spring-damper system. Viscous air damping is the dominant dissipation mechanism at atmospheric pressure. The beams in the folded flexure expand outward to relieve residual stress in the film, and inhibit buckling. The resonator is driven in the preferred ($x$) direction by electrostatic comb-finger actuators that are symmetrically placed on the sides of the shuttle. The suspension is designed to be compliant in the $x$ direction of motion and to be stiff in the orthogonal direction ($y$) to keep the comb fingers aligned.

## 3: Circuit-Level MEMS Representation

Our prior work on the NODAS circuit-level representation incorporated nodes for displacement and rigid-body position [6][20][21]. All suspended structures respond to inertial forces, so models should include these effects. Inertial sensors respond to acceleration and rotation with respect to a fixed frame of reference $(X, Y, \Theta)$, whereas the transducers detect displacement relative to the package, or chip, frame of reference $(x, y, \theta)$. On-chip actuation also acts relative to the chip frame of reference. The relationship between the two frames is shown in Fig. 2. The layout position of each element in the fixed frame is necessary to include in behavioral models for calculation of rotational inertial forces, such as centripetal and Coriolis forces.

Including rigid-body position in the nodal analysis allows users to build new designs without manually calculating the layout position of each element. Instead, the simulator calculates the layout position through the dc analysis. However, the initial approach in NODAS has two major drawbacks. First, the extra position nodes enlarge the solution matrix and slow down the simulation. Second, representing external steady-state acceleration (*e.g.,* gravity) in terms of an equivalent time-varying position produces large nodal position values after long transient simulation times and leads to an ill-conditioned specification of the problem. To solve this problem, microgyroscope circuit models developed by Lorenz *et al.* [10] specify initial layout position of each element as a static parameter specified by the user.

Our most recent NODAS representation, illustrated in Fig. 3 for a simple cantilever beam, combines the benefits of our previous representation and Lorentz' representation. The designer first creates a layout-based schematic using the icons as in Fig. 3(b). Values of the across variables from d.c. simulation are the layout positions of the elements. The through variables corresponding to the layout position nodes have no physical meaning. A script automates the generation of a second schematic for behavioral simulation, shown in Fig. 3(c), which includes the layout position values and eliminates potential entry errors by the user. In-plane displacements $(\delta x, \delta y, \delta\theta)$ are defined as across variables, and forces and torques $(F_x, F_y, M_\theta)$ acting on the element are through variables. The 50% reduction of mechanical nodes from our prior models provides more rapid simulation.

Sign conventions are essential for physically interpreting the simulation results. The $\delta x$ and $\delta y$ across variables are positive in the positive-axis directions and $\delta\theta$ is positive in a counterclockwise rotation (right-hand rule) around the positive $z$ axis. Through variables going *into* a node are interpreted as providing force in the positive-axis direction or providing torque in a counterclockwise rotation around the positive $z$ axis. The sign convention for through variables is illustrated in Fig. 3 at port *b*. (The term "port" denotes the four nodes associated with a physical point on an element.)

Behavioral models for the mechanical elements are based on theory of structural analysis [22] and are given in explicit detail in [6]. The current implementation includes four basic elements: the straight beam, rigid plate, electrostatic comb-finger actuator, anchor, and reference. Forces and moments are calculated in the local frame of reference of each instance of an element and then transformed into the chip frame of reference for addition to the through variables using a static rotational matrix, $[T]$. The anchor model sets displacement to zero. The reference model sets the origin of the coordinate system.

A straight beam is modeled as a linear spring element with a stiffness matrix, $[k]$, found by direct solution of the beam bending equation. Inertial force is modeled with a mass matrix, $[m]$, found by assuming static shape functions which link acceleration at the nodes to the distributed force along the beam. Damping is modeled as Couette air damping with damping matrix, $[B]$. The force variables in the local frame are

$$\left[F_{beam}\right] = \left[m\right]\left[\ddot{x}\right] + \left[B\right]\left[\dot{x}\right] + \left[k\right]\left[x\right] \qquad (1)$$

where $[x] = [T]^{-1}[\delta x_a\ \delta y_a\ \delta\theta_a\ \delta x_b\ \delta y_b\ \delta\theta_b]^{\mathrm{T}}$ are the displacements at beam's nodes *a* and *b*. The through variables for the forces and moments in the chip frame are given by $[F_{x,a}\ F_{y,a}\ M_a\ F_{x,b}\ F_{y,b}\ M_b]^{\mathrm{T}} = [T][F_{beam}]$. In contrast to current

through electrical elements, the through variables for forces and moments at external node *a* are not necessarily the same value as corresponding values at node *b*.

Plates are treated as rigid bodies, so the inertial mass for translational motion is simply equal to the material density times the plate volume. Damping is modeled as Couette air damping, which is proportional to the area of the plate [23]. The plate force variables are

$$\left[F_{plate}\right] = \left[m_p\right]\left[\ddot{x}\right] + \left[B_p\right]\left[\dot{x}\right] \tag{2}$$

where $[x] = [\delta x_m\ \delta y_m\ \delta\theta_m]^T$ is the displacement at the center of mass of the plate and $[F_{plate}] = [F_{x,m}\ F_{y,m}\ M_m]^T$ is the corresponding vector of rigid-body forces and moments.

Lateral electrostatic actuator models are based on nonlinear analytic equations for air-gap capacitance across the actuator electrodes. A first-order model assumes a parallel-plate sidewall capacitance,

$$C = \frac{\varepsilon A_{eff}}{g([x])} \tag{3}$$

where $A_{eff}$ is the effective electrode area including fringing field effects, and $g$ is the air gap expressed as a function of electrode displacement. The electrostatic force between the two electrodes is

$$\left[F_e\right] = \frac{1}{2}\left[\frac{\partial C}{\partial x_i}\right]v^2 \tag{4}$$

where $x_i$ are the individual terms in $[x]$ at the actuator's nodes *a* and *b*. The matrix terms are calculated in the actuator's local frame. The actuator model also includes rigid-body mass and damping terms, similar to the plate model.

## 4: Simulation Results

### 4.1: Microresonator

A layout-based schematic of the folded-flexure microresonator is shown in Fig. 4. The folded-flexure suspension is partitioned into 14 beam elements, and the central shuttle mass is partitioned into five plate elements. The comb-finger actuators are modeled as single elements. Each element serves both an electrical and mechanical role. A voltage source drives the lower actuator, while a dc bias voltage, $V_{dc}$, is applied to the moving structure. Displacement current ($i = V_{dc}\, dC/dt$) through the time-varying capacitance of the upper comb drive is sensed with a transresistance amplifier.

The behavioral models of the beam and plate are verified by comparing the behavioral simulation with finite-element results using 3-node beam elements in ABAQUS [24]. Static analysis of the shuttle displacement as a function of comb-drive voltage is performed through d.c. transfer-function analysis. The results, shown in Fig. 5, are within 0.26% of values generated using finite-element analysis. The $V^2$ nonlinearity of the force-displacement relation is readily apparent. The a.c. response of the resonator to a sinusoidal comb-drive voltage with a d.c. bias on the shuttle is given in Fig. 6. The fundamental resonant frequency matches within 1 % of finite-element simulation. The behavioral simulation also predicts a higher-order resonant mode.

### 4.2: Micromechanical Filter

A layout-based schematic of the micromechanical filter introduced by Nguyen [18] is shown in Fig. 7. Three folded-flexure microresonators, each having the same resonant frequency, are mechanically coupled together with beams connecting neighboring trusses. By choosing the size of the coupling beams appropriately, a narrow-band bandpass filter can be implemented. The filter is a good example of a hierarchically designed MEMS. The schematic was rapidly assembled by copying the pre-assembled resonator model three times and then adding the coupling beams. The narrow passband, shown in the ac analysis results in Fig. 8, compares well qualitatively with the SPICE model simulation based on Ngyuen's equivalent circuit model [18].

### 4.3: Lateral Crab-Leg Accelerometer

Microaccelerometers are composed of a suspended micromachined proof mass connected to a displacement sensor. The proof-mass displacement is directly proportional to external acceleration at frequencies well below self resonance. The lateral accelerometer shown in Fig. 9 is a plate mass connected to a "crab-leg" suspension. Each crab leg is created by joining two beams at 90°. Lateral (x-axis) displacement of the proof mass is sensed by the differential change in capacitance of two comb-finger arrays attached to opposing sides of the proof mass. The crab-leg accelerometer is similar to the microresonator in that both are suspended plate masses with attached comb-finger capacitors.

One important issue with accelerometer design is the determination of sensitivity to manufacturing variations. Geometric parameter values of beams and plates in the accelerometer schematic may be changed to determine their effect on output sensitivity and cross-axis sensitivity. For example, cross-axis sensitivity is explored by setting the width of the upper-right

crab-leg beam in Fig. 9 to be 10% smaller than the other flexural beams. Waveforms from a transient analysis are shown in Fig. 10. The on-axis external acceleration, $a_x$, is set to a 10 ms, 1 g pulse. After 10 ms, the plate responds to an overlapping 10,000 g pulse in cross-axis acceleration, $a_y$. The electrical effects of the cross-axis displacement of the plate are cancelled to first order by the balanced capacitive bridge formed from the two comb-finger sensors. However, the imbalance in the flexure causes the plate to move along the x-axis in response to the cross-axis acceleration. This displacement propagates through the sense amplifier and demodulator, and ultimately appears as undesirable cross-axis coupling at the output of the filter. Most circuit simulators have Monte Carlo simulation capability so that a scatter plot of sensitivities from random manufacturing variations can be automatically generated.

The elimination of the rigid-body position nodes in the new models greatly speeds up simulations that involve external acceleration. Simulation times are about 60% faster for a.c. analysis and 70% faster for transient analysis. The transient response in Fig. 10 (71 nodes) was completed in 3 minutes on an 200 MHz Ultrasparc 2 workstation with 256 MB RAM.

## 5: Conclusions

Structured design methods for suspended MEMS promise to shorten the development cycle to days, and enable design of more complex systems comprised of hundreds to thousands of micromechanical elements. Identification of reusable hierarchical representations of MEMS components is a critical first step in advancing toward a structured design methodology and in leveraging existing CAD tools.

A hierarchical circuit representation of MEMS down to a low level (equivalent to transistor level electronic design) enables quick evaluation of complex components by interconnecting schematic icons of beams and plates that are backed by behavioral models. Coupling the methodology with existing schematic capture tools that are compatible with electrical circuit analysis enables quick and efficient design of integrated MEMS. An important feature is the layout-based schematic, which provides an intuitive interface for the designer, and provides a path for direct generation of mask layout.

MEMS elements with geometrically parameterized models are very useful in evaluating the influence of manufacturing variations. The built-in variational analysis features in commercial behavioral simulators become important tools to evaluate manufacturability of MEMS designs. An expanded basis set of MEM devices with refined, second-order models will be developed as more designers adopt the hierarchical circuit methodology for MEMS.

## Acknowledgment

The authors thank former students Jan E. Vandemeer and Michael S. Kranz for their seminal work on the NODAS behavioral simulation and model generation. Discussions with Dr. Tamal Mukherjee are gratefully acknowledged.

## References

[1] J.M. Karam, B. Courtois, K. Hofmann, A. Poppe, M. Rencz, M. Glesner, V. Szekely, “Micro-systems Modeling at a System Level”, *APCHDL ‘96,* Bangalore, India, 8-10 January, 1996.

[2] *MEMCAD Web Page,* http://www.memcad.com, Microcosm Technologies, Inc., 201 Willesden Dr., Cary, NC 27513.

[3] *Intellisense Web Page,* http://www.intellis.com, IntelliSense Corporation, 16 Upton Dr., Wilmington, MA 01887.

[4] J. M. Funk, J. G. Korvink, J. Bühler, M. Båchtold, and H. Baltes, “SOLIDIS: A Tool for Microactuator Simulation in 3-D,” *J. of Microelectromech. Sys.*, v. 6, no. 1, pp. 70-82, March 1997. (*SOLIDIS Web Page,* http://www.ise.ch/solidis)

[5] L. D. Gabbay and S. D. Senturia, “Automatic Generation of Dynamic Macro-Models using Quasistatic Simulations in Combination with Modal Analysis,” *1998 Solid-State Sensors and Actuators Workshop,* Hilton Head Is., SC, June 7-11, 1998, pp. 197-200.

[6] J. Vandemeer, M.S. Kranz, and G. K. Fedder, “Hierarchical Representation and Simulation of Micromachined Inertial Sensors,” *1998 Int. Conf. on Modeling and Simulation of Microsystems, Semiconductors, Sensors and Actuators (MSM ‘98),* Santa Clara, CA, April 6-8, 1998.

[7] I. Getreu, “Behavioral Modelling of Analog Blocks using the SABER Simulator,”, Proc. Microwave Circuits and Systems, pp 977-980, August 1989.

[8] J. Clark, N. Zhou, S. Brown and K.S.J. Pister, “Nodal Analysis for MEMS Simulation and Design”, *1998 Int. Conf. on Modeling and Simulation of Microsystems, Semiconductors, Sensors and Actuators (MSM ‘98),* Santa Clara, CA, April 6-8, 1998.

[9] J. V. Clark, N. Zhou, S. Brown and K.S.J. Pister, “MEMS Simulation Using SUGAR v0.5”, *1998 Solid-State Sensors and Actuators Workshop,* Hilton Head Is., SC, June 7-11, 1998, pp.191-196.

[10] G. Lorenz and R. Neul, “Network-Type Modeling of Micromachined Sensor Systems,” *1998 Int. Conf. on Modeling and Simulation of Microsystems, Semiconductors, Sensors and Actuators (MSM ‘98),* Santa Clara, CA, April 6-8, 1998.

[11] D. Teegarden, G. Lorenz and R. Neul, “How to Model and Simulate Microgyroscope Systems,” *IEEE Spectrum*, pp. 67-75, July 1998.

[12] Tanner Research, Inc., 2650 E. Foothill Blvd., Pasadena, CA, 91107, http://www.tanner.com.

[13] *ADXL50 Accelerometer Data Sheet,* Analog Devices, Inc., One Technology Way, P.O.Box 9106, Norwood, MA 02062-9106, 1996 (http://www.analog.com).

[14] *MMAS40G10D Accelerometer Data Sheet,* Motorola Sensor Products, 1996 (http://design-net.com/senseon).

[15] M. A. Mignardi, “Digital Micromirror Array for Projection TV,” *Solid State Technology,* v.37, no.7, pp. 63-4, July 1994.

[16] D. A. Koester, R. Mahadevan, K. W. Markus, *Multi-User MEMS Processes (MUMPs) Introduction and Design Rules*, available from MCNC MEMS Technology Applications Center, 3021 Cornwallis Road, Research Triangle Park, NC 27709, rev. 3, Oct. 1994, 39 pages.

[17] W. C. Tang, T.-C. H. Nguyen, M. W. Judy, and R. T. Howe, “Electrostatic comb drive of lateral polysilicon resonators,” *Sensors and Actuators A*, vol.21, no.1-3, pp. 328-31, Feb. 1990.

[18] K. Wang and C. T.-C. Nguyen, “High-Order Micromechanical Electronic Filters,” *IEEE MEMS Workshop,* Nagoya, Japan, January 26-30, 1997, pp. 25-30.

[19] M. J. Daneman, N. C. Tien, O. Solgaard, K. Y. Lau, and R. S. Muller, “Linear Vibromotor-Actuated Micromachined microreflector for Integrated Optical Systems, *1996 Solid-State Sensors and Actuators Workshop,* Hilton Head Is., SC, June 2-6, 1996, pp. 109-112.

[20] J. Vandemeer, M.S. Kranz, and G. K. Fedder, “Nodal Simulation of Suspended MEMS with Multiple Degrees of Freedom,” *1997 Int. Mechanical Engineering Congress and Exposition: The Winter Annual Meeting of ASME in the 8th Symposium on Microelectromechanical Systems (DSC-Vol.62)*, Dallas, TX, 16-21 November, 1997, pp. 113-118.

[21] http://www.ece.cmu.edu/~mems/nodas.html

[22] S. P. Przemieniecki, *Theory of Matrix Structural Analysis,* McGraw-Hill, New York, New York, 1968.

[23] X. Zhang and W. C. Tang, “Viscous Air Damping in Laterally Driven Microresonators,” *Sensors and Materials,* v. 7, no. 6, pp.415-430, 1995.

[24] *ABAQUS Web Page,* http://www.hks.com, Hibbitt, Karlsson, and Sorensen, Inc., 1080 Main Street, Pawtucket, RI 02860.

## Figure Captions

Fig. 1. A folded-flexure comb-drive microresonator fabricated in a polysilicon surface microstructural process. (a) Layout. (b) Cross-section *A-A'*.

Fig. 2. Fixed frame of reference $(X, Y, \Theta)$ and chip frame of reference $(x, y, \theta)$.

Fig. 3. Circuit-level representation of a simple cantilever beam with in-plane layout position $(X, Y, \Theta)$ and displacements $(\delta x, \delta y, \delta\theta)$. (a) Physical view. (b) Layout-based schematic. (b) Behavioral schematic.

Fig. 4. Layout-based schematic of the folded-flexure comb-drive microresonator shown in Figure 4. Parameter values are listed next to the element symbol.

Fig. 5. Static analysis of microresonator displacement as a function of applied voltage. Results from finite-element static analysis using beam elements are plotted for comparison.

Fig. 6. Frequency response of the micro-resonator displacement. The second-order response derived from finite-element static and modal analysis is plotted for comparison.

Fig. 7. Layout-based schematic of a micro-mechanical bandpass filter made from three coupled folded-flexure resonators.

Fig. 8. Micromechanical filter simulation. The dip in the passband is from tuning mismatch in the coupling beams.

Fig. 9. A crab-leg lateral capacitive accele-rometer design. (a)Layout-based schematic with electronics represented as functional blocks. (b) Simplified layout of the transducer (rotated by 90°).

Fig. 10. Transient response of displacement and output voltage to pulses in external acceleration.

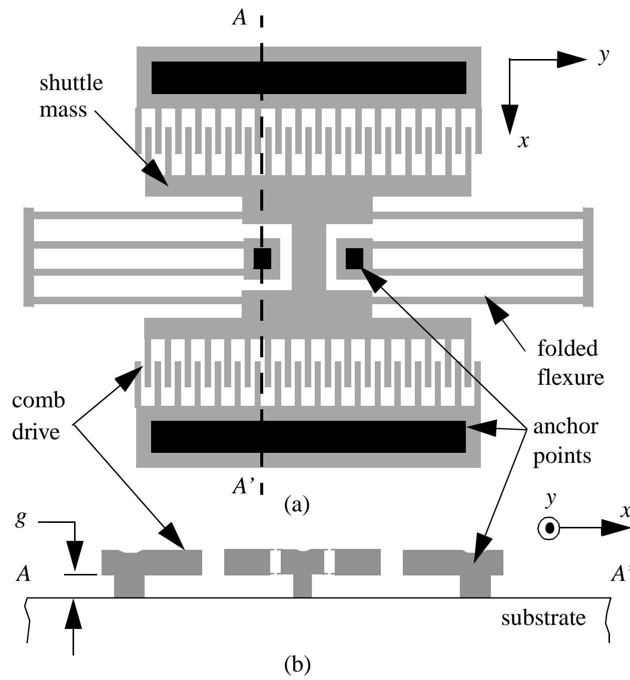


Fig. 1. A folded-flexure comb-drive microresonator fabricated in a polysilicon surface microstructural process. (a) Layout. (b) Cross-section *A*-*A'*.

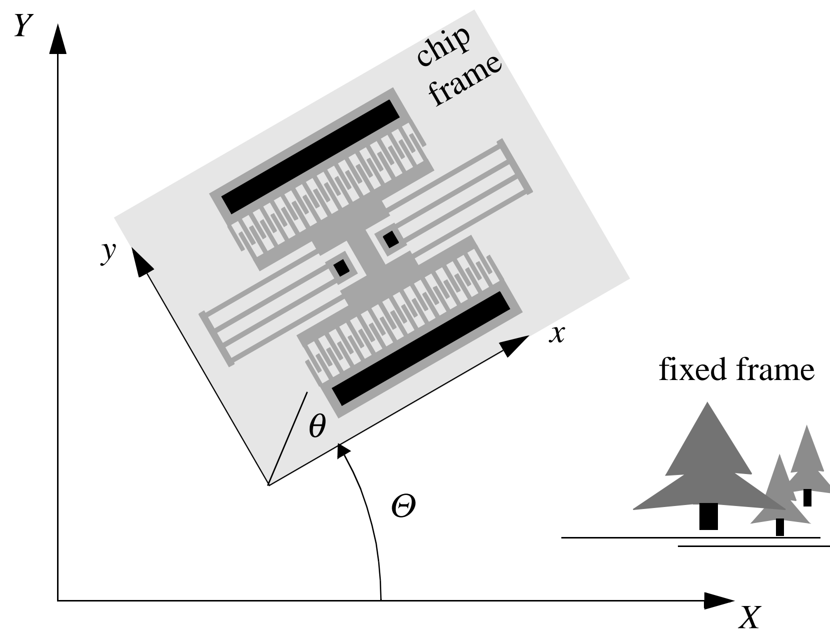


Fig. 2. Fixed frame of reference *(X, Y, Θ)* and chip frame of reference *(x, y, θ)*.

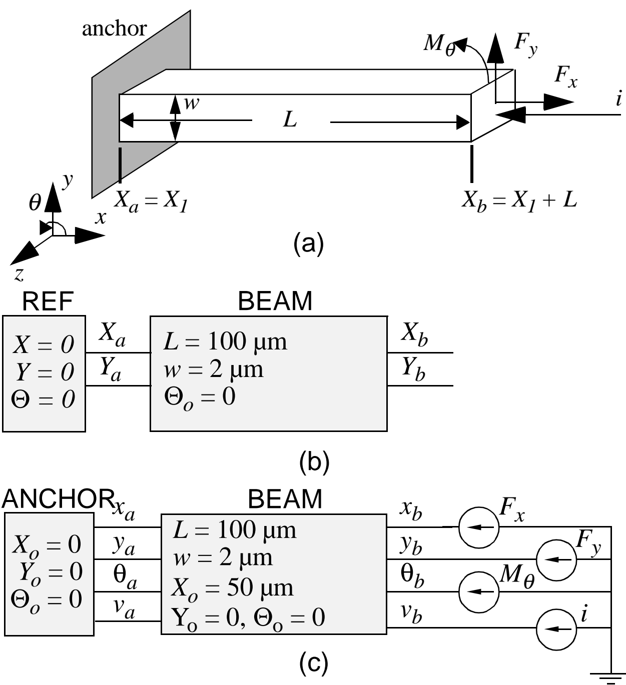


Fig. 3. Circuit-level representation of a simple cantilever beam with in-plane layout position *(X, Y, Θ)* and displacements *(δx, δy, δθ)*. (a) Physical view. (b) Layout-based schematic. (b) Behavioral schematic.

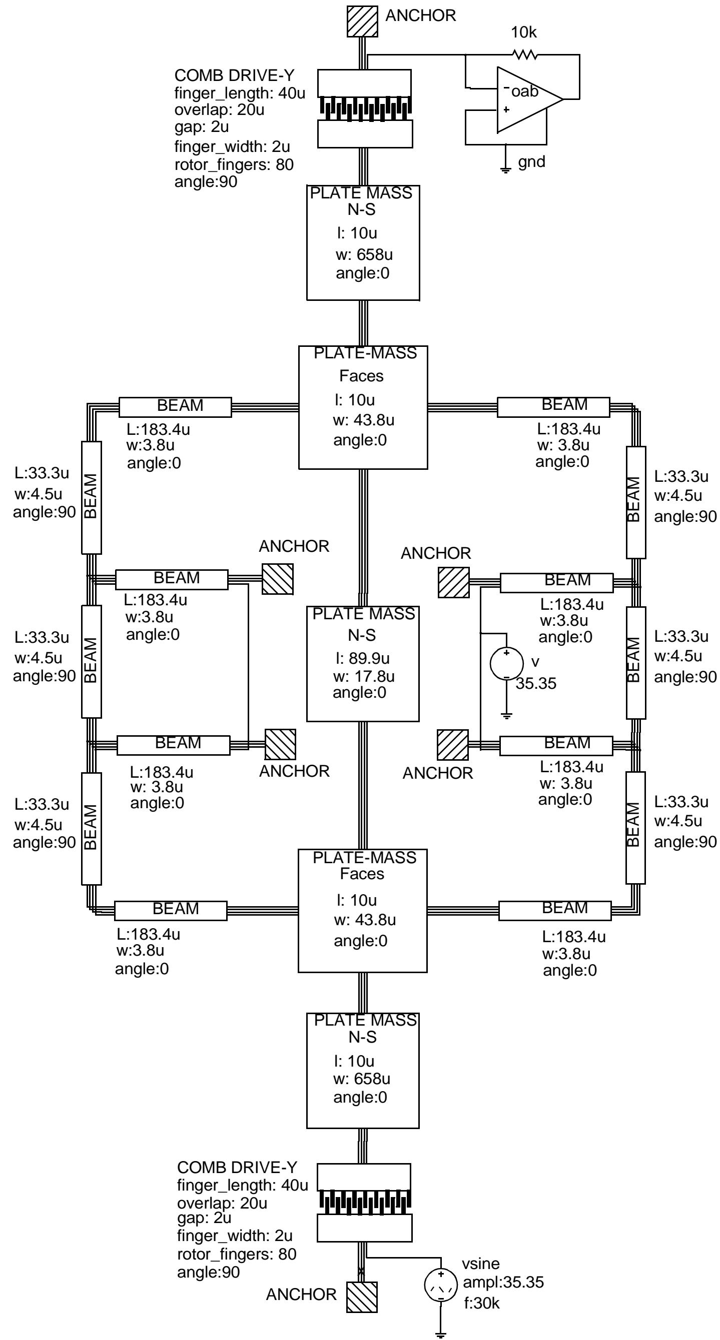


Fig. 4. Layout-based schematic of the folded-flexure comb-drive microresonator shown in Figure 4. Parameter values are listed next to the element symbol.

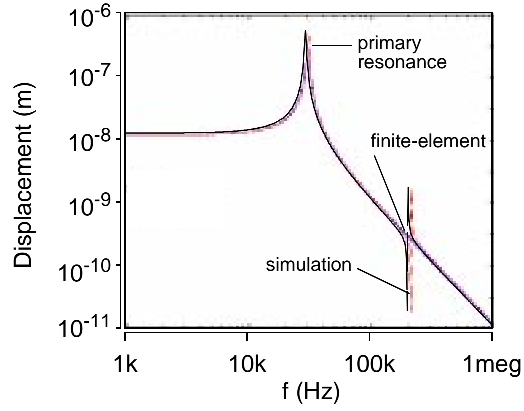


Fig. 6. Frequency response of the micro-resonator displacement. The second-order response derived from finite-element static and modal analysis is plotted for comparison.

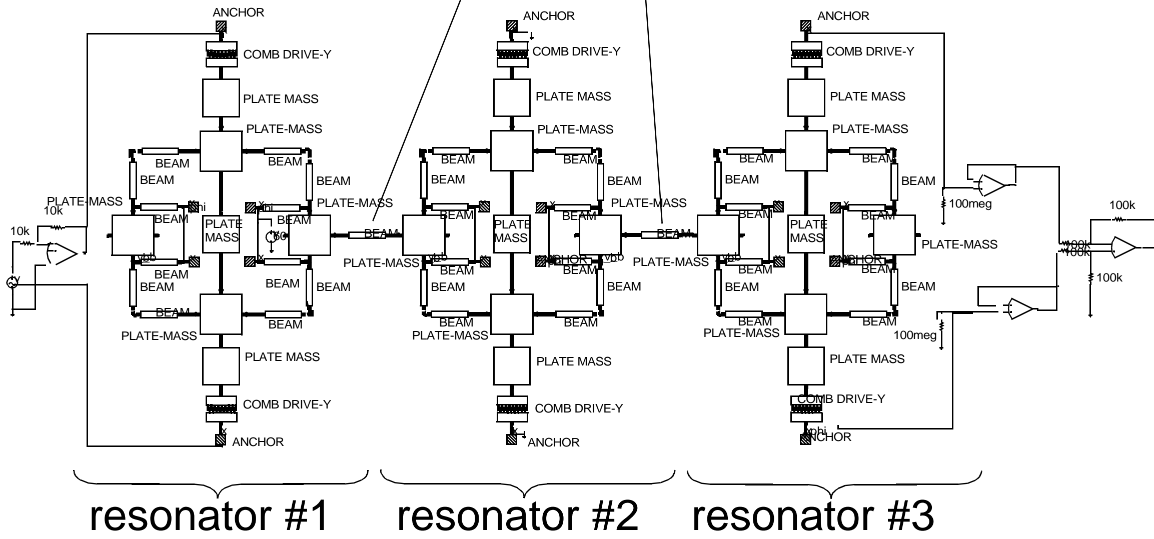


Fig. 7. Layout-based schematic of a micro-mechanical bandpass filter made from three coupled folded-flexure resonators.

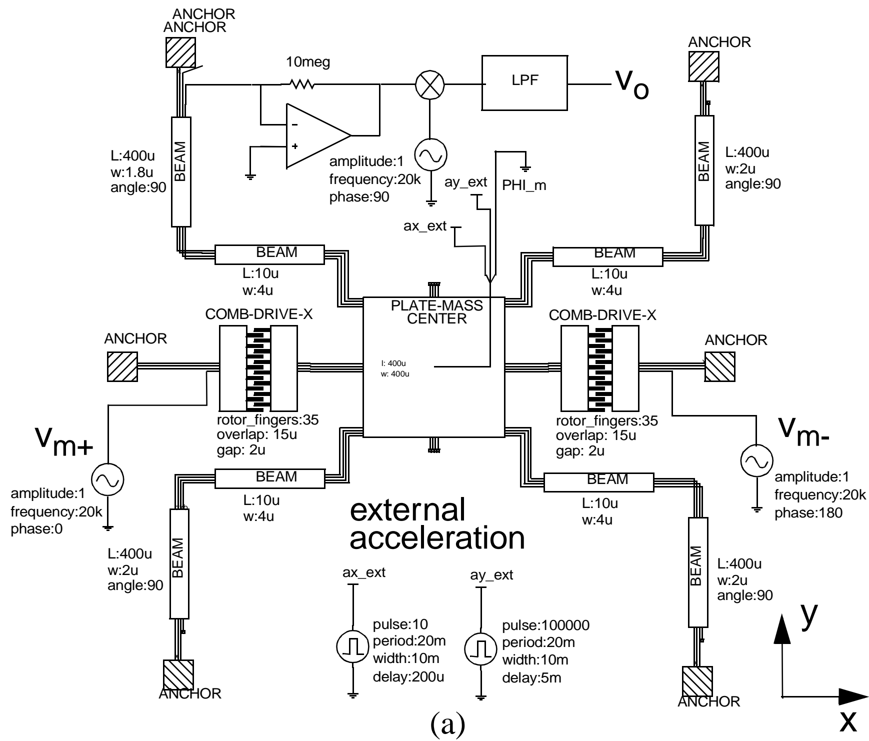


(a)

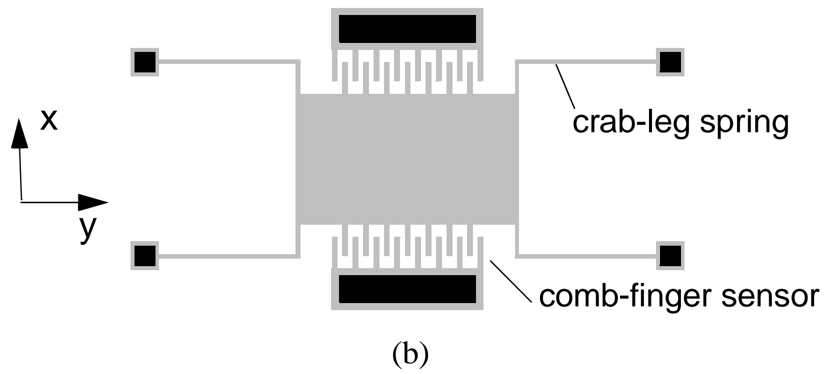


(b)

Fig. 9. A crab-leg lateral capacitive accele-rometer design. (a)Layout-based schematic with electronics represented as functional blocks. (b) Simplified layout of the transducer (rotated by 90°).

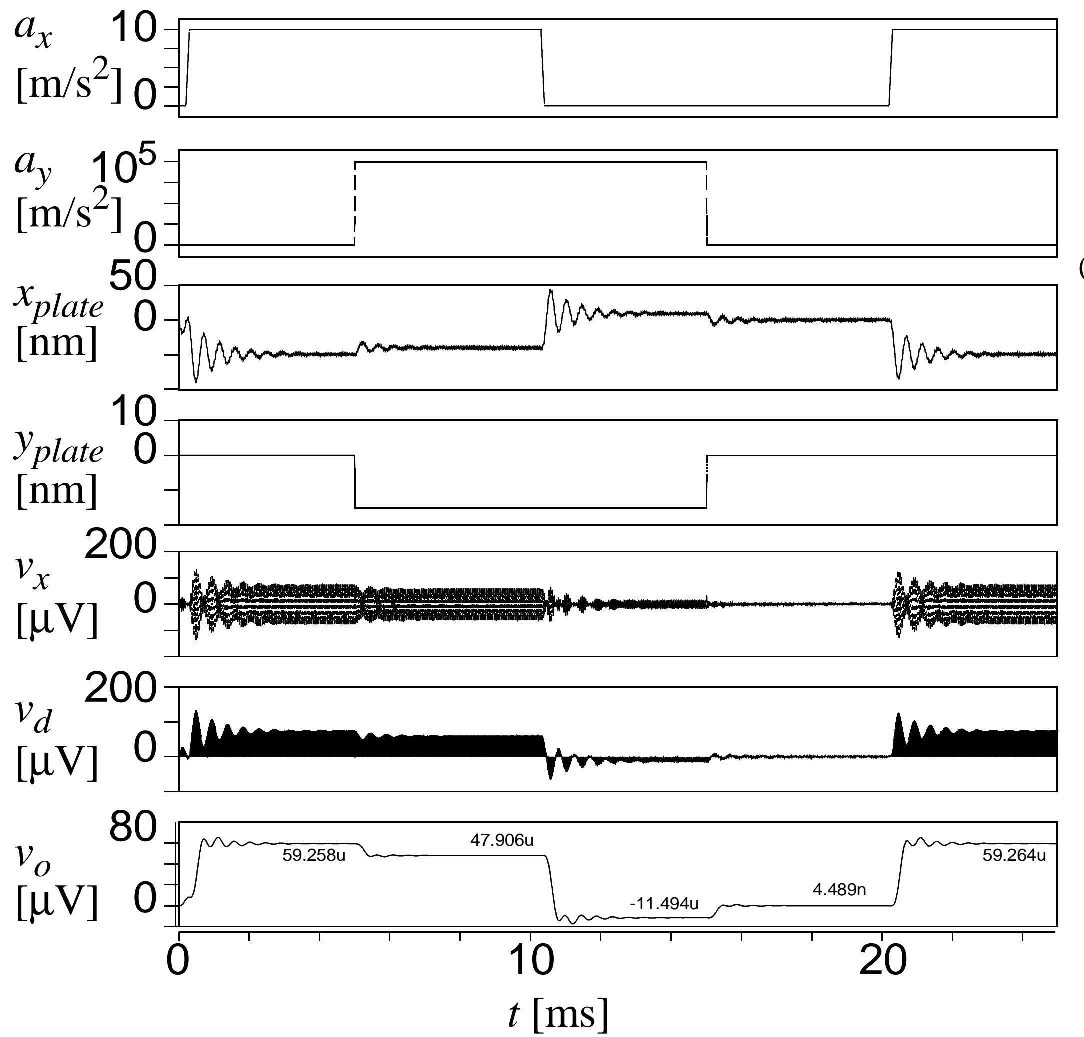


Fig. 10. Transient response of displacement and output voltage to pulses in external acceleration.